JOURNAL OF MATERIALS SCIENCE 23 (1988) 4049–4058

The effect of boron on the microstructure and physical properties of chemically vapour deposited nickel films

A. N. CAMPBELL, A. W. MULLENDORE, C. R. HILLS
Sandia National Laboratories, Albuquerque, New Mexico 87185, USA

J. B. VANDERSANDE
Massachusetts Institute of Technology, Department of Materials Science and Engineering, Cambridge, Massachusetts 02139, USA

The solid solution addition of boron greatly enhances the strength and hardness of chemically vapour deposited (CVD) nickel while dramatically changing the microstructure. The solid solubility of boron in nickel is limited, and single-phase alloys containing in excess of 0.3 at % B are supersaturated with respect to the formation of one or more intermetallic boride phases. Single-phase Ni–B alloys containing 0 to 13.0 at % B were produced by CVD on polycrystalline copper substrates at 155° C in an atmospheric pressure process. The microstructure, mechanical and physical properties were characterized for the alloys both as-deposited and after various thermal treatments by using optical microscopy, transmission electron microscopy, X-ray diffraction and micro-indentation hardness testing with a diamond pyramid indentor. The grain size of the alloy was found to decrease sharply with rising boron content. Concomitantly, the defect density of the material rose significantly, the microhardness increased and the ductility decreased. With annealing at a temperature of 300° C or greater, precipitation of the Ni_3B intermetallic phase, recovery and grain growth occurred.

1. Introduction

The mechanical behaviour of chemically vapour deposited (CVD) nickel is significantly altered by the addition of boron. Addition of as little as 0.27 at % B has been shown to increase the alloy yield stress, ultimate tensile stress and hardness each by about 50% [1]. The enhancement of the mechanical properties of Ni–B alloys increases with boron content. The high hardness of these alloys suggests their application as wear-resistant coatings. Mullendore and Pope [2] have demonstrated that the wear resistance of Ni–B alloys increases with boron content and is excellent for alloys containing 13.0 and 37.0 at % B in pin-on-disc experiments where the pin was glass-filled epoxy.

The equilibrium solid solubility of boron in nickel is quite low, with a maximum of the order of 0.15 [3] to 0.3 at % [4] at the $Ni–Ni_3B$ eutectic temperature of 1093° C. The CVD Ni–B alloys are single-phase and therefore those containing more than about 0.1 at % B are metastable with respect to the formation of one or more intermetallic boride phases at ambient or somewhat higher temperatures.

Skibo and Greulich [1] studied the microstructure and mechanical properties of metastable Ni–B alloys containing 0.23–1.08 at % B (0.05–0.2 wt %) made by the codeposition of nickel and boron from nickel tetracarbonyl, $Ni(CO)_4$ and diborane, B_2H_6 in a CVD reactor. The increase in strength and hardness of the as-deposited alloys with rising boron content noted in their work was accompanied by a decrease in ductility. An anneal of 4 h at a temperature between 400 and 800° C was found to decrease the hardness and strength of the alloys somewhat relative to the as-deposited condition while leading to improved toughness. Precipitation of an intermetallic boride phase identified as Ni_2B was reported to occur during annealing.

In the present work the behaviour of Ni–B alloys spanning a broader range of boron contents, from 0 to 13 at %, was investigated. The microstructures and phases present in both the as-deposited and annealed material were characterized by using transmission electron microscopy (TEM), including imaging and selected area diffraction, and X-ray diffraction (XRD). The mechanical behaviour was described in terms of the room temperature microhardness. In a parallel study, the thermal behaviour of the alloys was investigated with differential scanning calorimetry (DSC) [5].

2. Experiments

The Ni–B deposits were prepared by codeposition of nickel and boron in a CVD reactor from $Ni(CO)_4$ and B_2H_6. The reaction chamber is shown schematically in Fig. 1. The $Ni(CO)_4$ was metered as a liquid and vapourized in a heated line with added CO. The B_2H_6 was diluted with argon and mixed with the $Ni(CO)_4$ and CO. The gas mixture was introduced into the reaction chamber where deposition occurred on a

0022–2461/88 $03.00 + .12

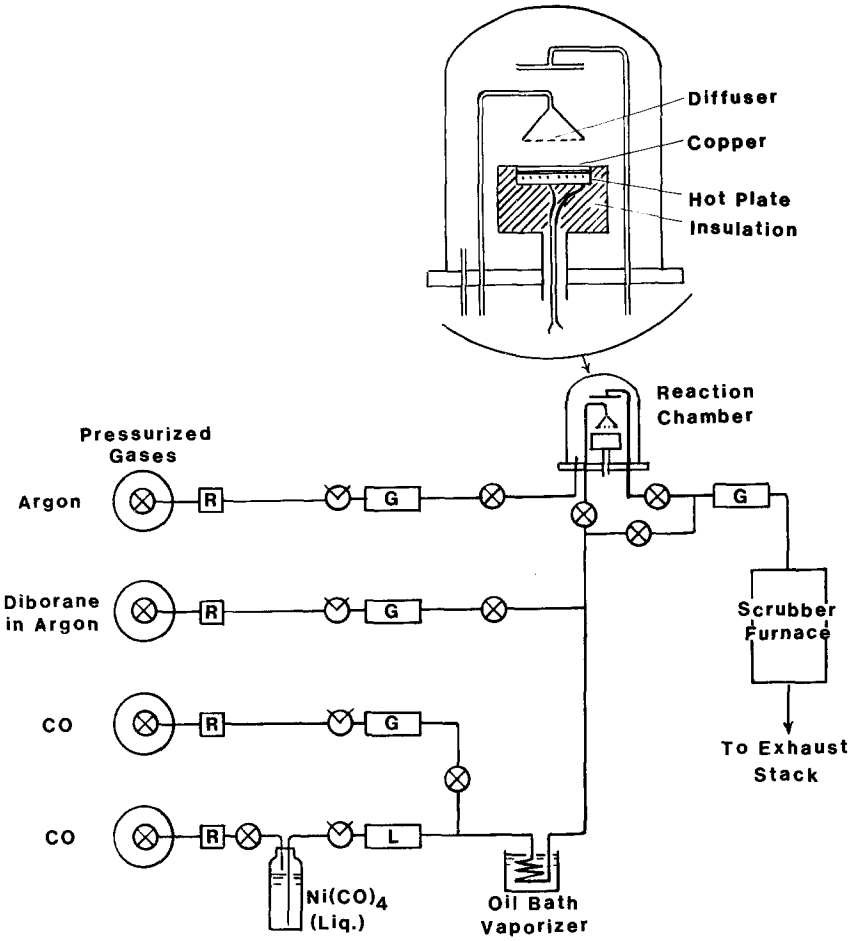

Figure 1 Schematic of the CVD reactor. (⊗) shut-off valve, (⊗) needle valve, R gas regulator, L Liquid flow meter, G gas flow meter).

polycrystalline copper substrate resistively heated to 155° C. Pure nickel deposits were prepared in the same way without the addition of B_2H_6. Layered deposits, in which the boron content was increased incrementally during deposition by adjusting the flows of $Ni(CO)_4$ and B_2H_6 were produced for use as boron concentration calibration standards. The deposit produced consisted of layers containing 0, 1.0, 2.5, 3.5 and 5 at % B, each approximately 0.15 mm in thickness. The furnace exhaust was passed through two getter furnaces to remove the unreacted $Ni(CO)_4$ prior to venting to the atmosphere. The pressure in the reaction chamber was ambient (about 650 torr). Pure nickel and Ni–B alloys were deposited at a rate of approximately 0.15 mm h^{-1}. The deposit thicknesses ranged from 0.03 to 0.5 mm. The deposits did not adhere strongly to the copper substrates and were thus easily removed.

TEM specimens were prepared from the as-deposited and annealed (in purified argon) nickel and Ni–B alloys. Prior to jet-electropolishing the pure nickel specimens were thinned to about 0.1 mm by hand grinding with 600 grit emery paper. The Ni–B deposits, initially only about 0.1 mm thick, did not require pretreatment. Discs punched from the pure Ni and Ni–B deposits were thinned by using a 10–20 vol % $HClO_4$/balance methanol solution at less than −50 to −25° C in a Fischione dual-jet electropolishing cell operated at a potential of 22.5–25 V d.c.

The microhardness was measured on the cross-section of a Ni–B layered deposit. The layered material was mounted in epoxy resin, polished and etched. Microhardness indentations were made across the entire specimen by using a diamond pyramid indentor and a load of 100 g. Vickers hardness as a function of boron content is reported for the as-deposited and annealed specimens.

Several other analytical techniques were used to characterize the nickel and Ni–B deposits. The specimens were examined by using standard X-ray diffractometer techniques with Cu$K\alpha$ radiation and, in addition, texture analysis of the pure nickel material was performed. DSC was performed with a Perkin–Elmer DSC-2. Compositional analysis of the Ni–B films was accomplished by using sputter-profiling in an Auger system and inductively coupled plasma (ICP) spectroscopy.

3. Results and discussion

3.1. Pure nickel films

The pure nickel films were found to have the largest grain size and simplest microstructure of the deposits observed. Fig. 2 is a typical bright field transmission electron micrograph of the nickel in the plane of the film. The thinned area observed lies approximately in the middle of the 0.5 mm thickness of the specimen. The grain size distribution is bimodal. The microstructure consists of approximately equal area fractions of large, relatively defect-free grains 1.0–3.0 μm in diameter and significantly finer grains, approximately 0.1 μm in size and containing a significantly higher defect density. Similar observations were made by Grovenor *et al.* [6] for nickel films 9–14 μm in thickness formed by electron-beam evaporation. Selected area electron diffraction indicated that the large grains are typically in the ⟨0 1 1⟩ orientation. This result was

Figure 2 Microstructure of CVD pure nickel.

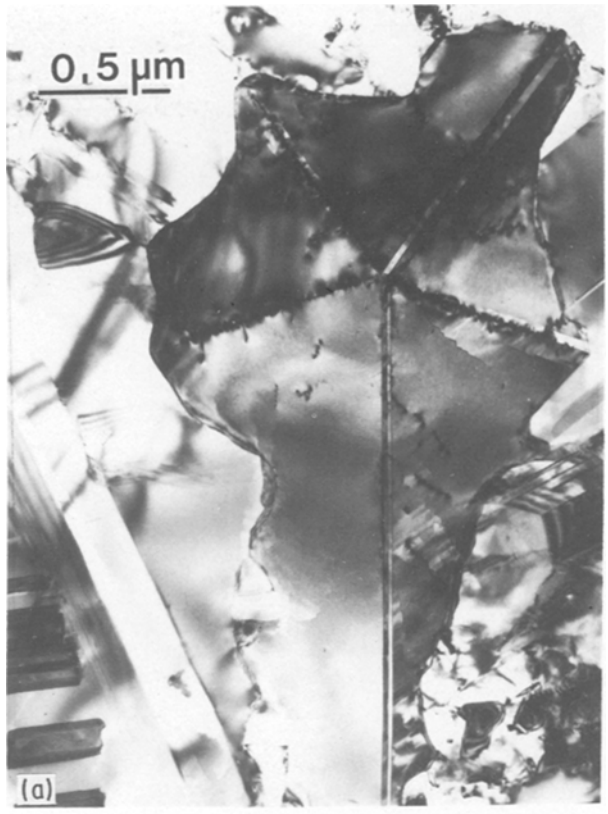

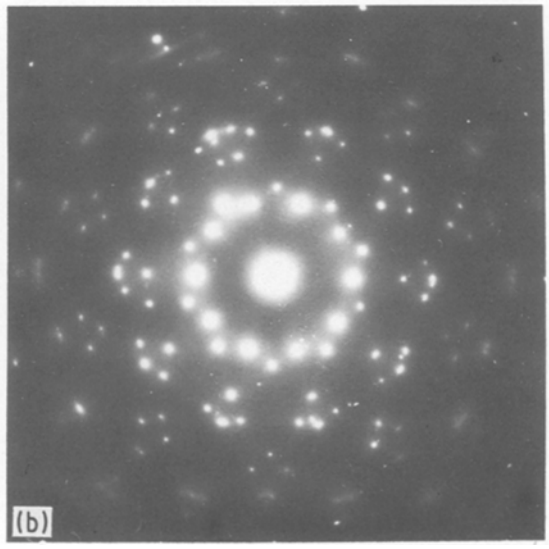

Figure 3 (a) Five ⟨0 1 1⟩ grains meet to form a pentagon. (b) Zone axis diffraction pattern of the pentagon.

confirmed by an X-ray texture analysis which indicated that the deposits have a slight ⟨0 1 1⟩ texture and that the area density of the ⟨0 1 1⟩ material is about 2.5 times that which would be expected if the structure were completely random.

A rather unusual feature of the microstructure is the meeting of five of the large ⟨0 1 1⟩ grains at 72° angles to form a pentagon, as shown in Fig. 3a. It was estimated from 20 randomly taken micrographs at 20 000 × that the area fraction of the pentagons is 0.08–0.10. The zone axis diffraction pattern (ZADP) of the entire pentagon displays near five-fold symmetry (Fig. 3b). The crystallography of the arrangement suggests that the fine grains are twin-related. In the fcc crystal structure the twin planes are {1 1 1}, and two sets of such planes exist parallel to the ⟨0 1 1⟩ direction with 70.5° between them. However, a careful analysis of the ZADP produced by the pentagons [7] shows that these features are not produced by twinning. The ZADP calculated for fine ⟨0 1 1⟩ fcc twin-related grains, Fig. 4a, is very different from that of the pentagon and displays only two-fold symmetry. By contrast, Fig. 3b is reproduced almost exactly by the ZADP calculated for fine fcc ⟨0 1 1⟩ grains rotated by multiples of 72° with respect to each other about a common ⟨0 1 1⟩ axis, Fig. 4b [7, 8].

A mechanism for the formation of this microstructural feature is suggested by Yang [9]. It has been shown that in the early stages of vapour deposition of gold (also fcc) small clusters of atoms 5–20 nm in diameter form prior to the coalescence of the film [10]. Some of these clusters, having pentagonal profiles, are regular decahedra consisting of five identical tetrahedra. The crystal structure of the tetrahedral units is metastable body-centred orthorhombic (bco), produced by a small distortion of the fcc structure. Such a distortion required only small displacements of the individual atoms, but the result is that the $\{1\,0\,1\}_{bco}$ planes, which correspond to the $\{1\,1\,1\}_{fcc}$, are separated by exactly 72°, rather than by 70.5° as are $\{1\,1\,1\}_{fcc}$. The geometry of the decahedron and the relationship between the fcc and bco structures are shown in Figs 5a and b. This suggests that the nickel grains which assume the pentagonal form arose from decahedral nuclei. As these clusters grew beyond a critical size, a few tens of nanometers [11], the bco (which was stabilized by a reduction in surface free energy at the smaller particle sizes) reverts to the stable fcc. The individual grains retain their original orientation relationship, and the mismatch at the

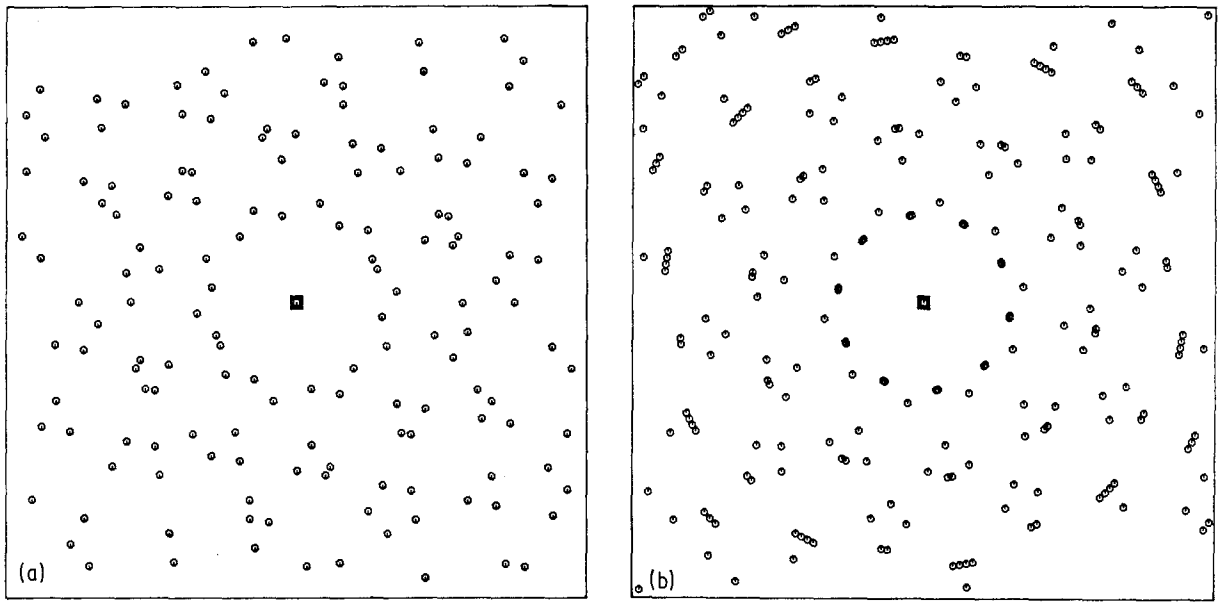

Figure 4 (a) Zone axis diffraction pattern calculated for 5 ⟨0 1 1⟩ twin-related grains. (b) Zone axis diffraction pattern calculated for 5 ⟨0 1 1⟩ grains rotated by multiples of 72° about a common ⟨0 1 1⟩ zone axis.

grain boundaries is taken up by secondary twins and dislocations which are visible in Fig. 3a.

An attempt was made to duplicate Yang's experiment [9] using nickel in place of gold. Specimens were prepared to study the early stages of deposition of nickel by depositing a very thin nickel layer on carbon substrates on copper grids. Partial coverage of the carbon film by nickel clusters about 300 nm in diameter was achieved. Selected area diffraction from the deposit gave a polycrystalline nickel pattern with no indication of the presence of the bco structure although some of the particles did appear to have pentagonal profiles. It is likely that the volume fraction of particles, either in this experiment or in Yang's gold particle work, that are decagonal is small and, in this case, may have been present in numbers too small to be revealed by electron diffraction. It is also possible that initially decagonal particles had already exceeded the critical size. High resolution work to examine the microstructure of the particles was not attempted.

3.2. Ni–B alloys

The addition of as little as 0.16 at % B to nickel leads to a considerably reduced grain size. The microstructure of Ni–0.16 at % B is shown in Fig. 6a. It is similar to that of pure nickel, Fig. 2, and contains some of the pentagonal features. However, the scale of the microstructure is reduced by a factor of about 2 (the largest grains are about 0.5–1.5 μm in diameter and the small grains are approximately 0.05 μm in size) and the defect density is appreciably higher as can be seen by comparing Figs 2 and 6a. The microstructure becomes even finer as the boron content is further increased, Figs 6b–d. The as-deposited grain sizes for nickel containing 0.16, 2.6, 5.3 and 13.0 at % B are given in Table I; the approximate diameters of both the large and small grains are given. A bimodal grain size distribution in nickel alloy specimens and the decrease in nickel grain size with alloy additions also have been observed in the Ni–Al system [6, 12].

The nickel and boron contents of the Ni–B alloys, with the exception of Ni–0.16 at % B, were determined by ICP analysis with an associated error of $\pm 2\%$ (relative). Sputter profiling was used to analyse the Ni–0.16 at % B specimen. The uncertainty in the latter measurement is high, $\pm 50\%$, because the alloys used as calibration standards for the Auger signals contain at least an order of magnitude more boron than the specimen. The presence of approximately 1 at % each

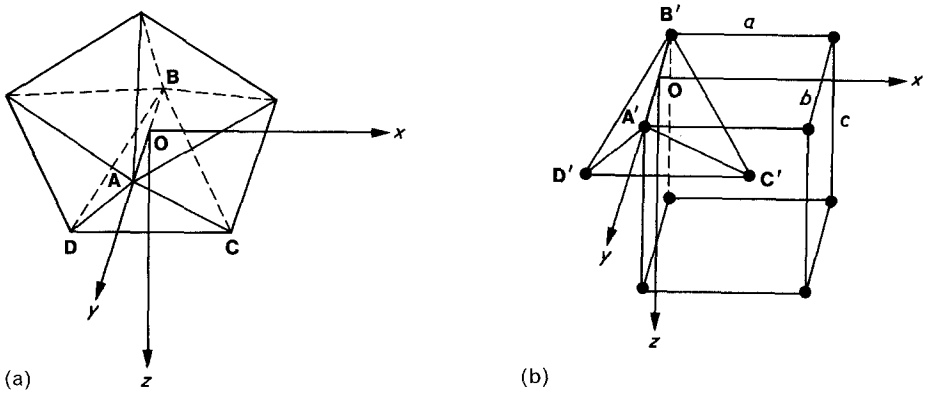

Figure 5 (a) A regular decahedron consisting of five irregular tetrahedra, such as ABCD. AC = AD = BC = BD, AB = 1.0515AC. (b) Relationship between the fcc and bco structures. The bco unit cell is shown with a unit tetrahedron A′B′C′D′ indicated. The lattice is fcc if $a = b$ and $c = \sqrt{2}a$. A′B′C′D′ is then a regular tetrahedron. With a small distortion of the fcc, the lattice becomes bco. The pertinent relationships for bco are $b = 1.0515a$ and $c = 1.3764a$. A′B′C′D′ is irregular and similar to ABCD in (a). (After Yang, [9].)

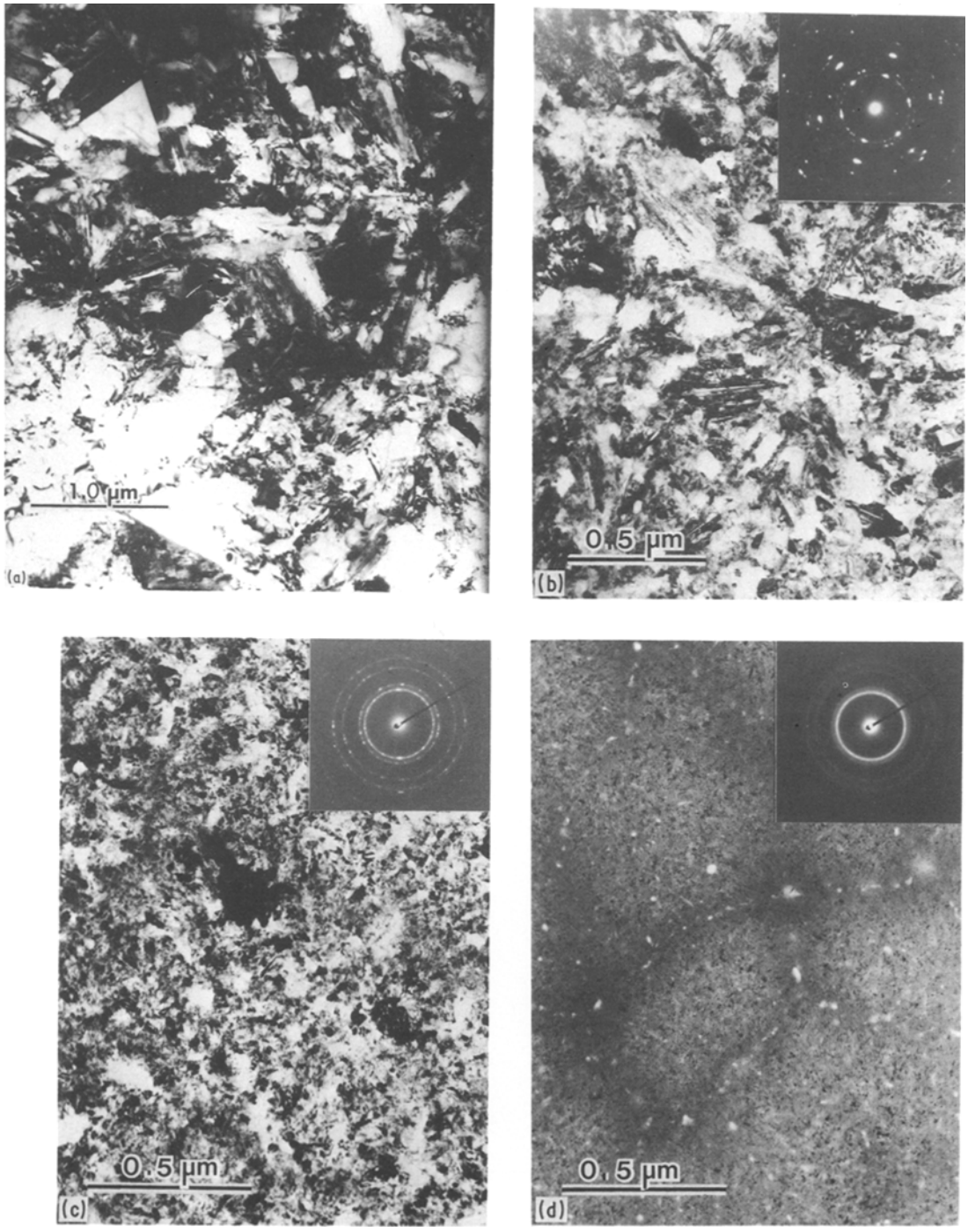

Figure 6 Bright field transmission electron micrographs of as-deposited (a) Ni–0.16 at % B, (b) Ni–2.6 at % B, (c) Ni–5.3 at % B, and (d) Ni–13.0 at % B alloys. All micrographs in the plane of the film.

of carbon and oxygen was observed by both combustion analysis and sputter profiling.

Bright field transmission electron micrographs of the Ni–B alloys are shown in Figs 6a–d. The pentagonal features found in pure nickel are still present in the Ni–0.16 at % B specimen, Fig. 6a, but they are not obvious in the alloys with higher boron contents. The large ⟨0 1 1⟩ grains are found in the Ni–0.16 and −2.6 at % B specimens but are not observed in the alloys containing more boron. By

TABLE I

Boron Content of alloy (at %)	Grain size, as-deposited		Grain size annealed 600° C for 25 h (μm)	Lattice parameter a_0 (nm)
	Large (μm)	Small (μm)		
0	1.0–3.0	0.1	–	$0.35212 \pm 1.2 \times 10^{-4}$
0.16	0.5–1.5	0.05	–	$0.35230 \pm 3.8 \times 10^{-5}$
2.6	0.1–0.5	–	0.23	$0.35140 \pm 1.3 \times 10^{-4}$
5.3	0.04–0.2	–	0.13	$0.35123 \pm 1.6 \times 10^{-4}$
13.0	0.01–0.03	–	0.20	–

addition of 13 at % boron to nickel the microstructure shown in Fig. 6d is obtained. The structure is single phase, and the dark regions are grains favourably oriented for diffraction. The grains are extremely fine, 0.01–0.03 μm in diameter. Selected area electron diffraction patterns included with Figs 6b–d indicate that the as-deposited alloys are single phase solid solutions based on the nickel f c c structure. The lines in the diffraction patterns become continuous and are broadened as the boron content rises, consistent with the observed decrease in grain size.

Fine voids are observed occasionally in the Ni–B deposits. The number density of voids, quite low in pure nickel and Ni–0.16 at % B, increases with the boron content as shown by Figs 6a–d. The void density is quite high in the Ni–13 at % B deposit, Fig. 6d. Large voids form the walls of a cellular superstructure in this alloy. The cells are approximately 1 μm in diameter and each encompasses many grains.

Void formation attributed to shadowing is commonly observed in materials formed by physical vapour deposition [13]. The elevated temperature of most CVD processes results in a sufficiently high surface mobility of the depositing species to preclude the entrapment of voids by the shadowing mechanism. However, the modest temperature (approximately 0.25 T_m, where T_m is the absolute melting temperature of nickel) and high rate of deposition in the Ni–B CVD process may permit the pinching off of voids by shadowing. The observation of columnar features which are of about the same width as the cells, 1 μm, by optical metallography of cross sections of the deposits supports the shadowing hypothesis. The somewhat irregular shape of the large voids found at cell boundaries is also suggestive of their formation by shadowing.

By contrast, the precipitation of excess vacancies generated during deposition is probably the mechanism of formation of the smaller voids found at the cell centres. It is possible that the larger voids found at the cell boundaries also form by nucleation and growth of vacancy clusters. However, it is not obvious why the large voids would nucleate and grow to form a columnar structure in an initially homogeneous matrix. It seems more likely that the voids at cell boundaries are formed by shadowing during deposition. Nucleation of new voids adjacent to the cell boundary would be suppressed as it is energetically more favourable for excess vacancies in that region to migrate to the large voids already in existence. The regions adjacent to the cell boundaries appear denuded of voids, which suggests that the excess vacancies in this region diffused to the large boundary voids.

It is not clear how the increased boron content leads to a greater number of voids in the deposits. The presence of boron may induce a larger concentration of excess vacancies or may decrease the surface mobility of the depositing species.

The solid solution of boron contracts the f c c nickel lattice. The measured lattice parameter, a_0, decreased from $0.35212 \pm 1.2 \times 10^{-4}$ nm for pure nickel to $0.35123 \pm 1.6 \times 10^{-4}$ nm for the Ni–5.3 at % specimen. The measured a_0 for pure nickel is in fairly good

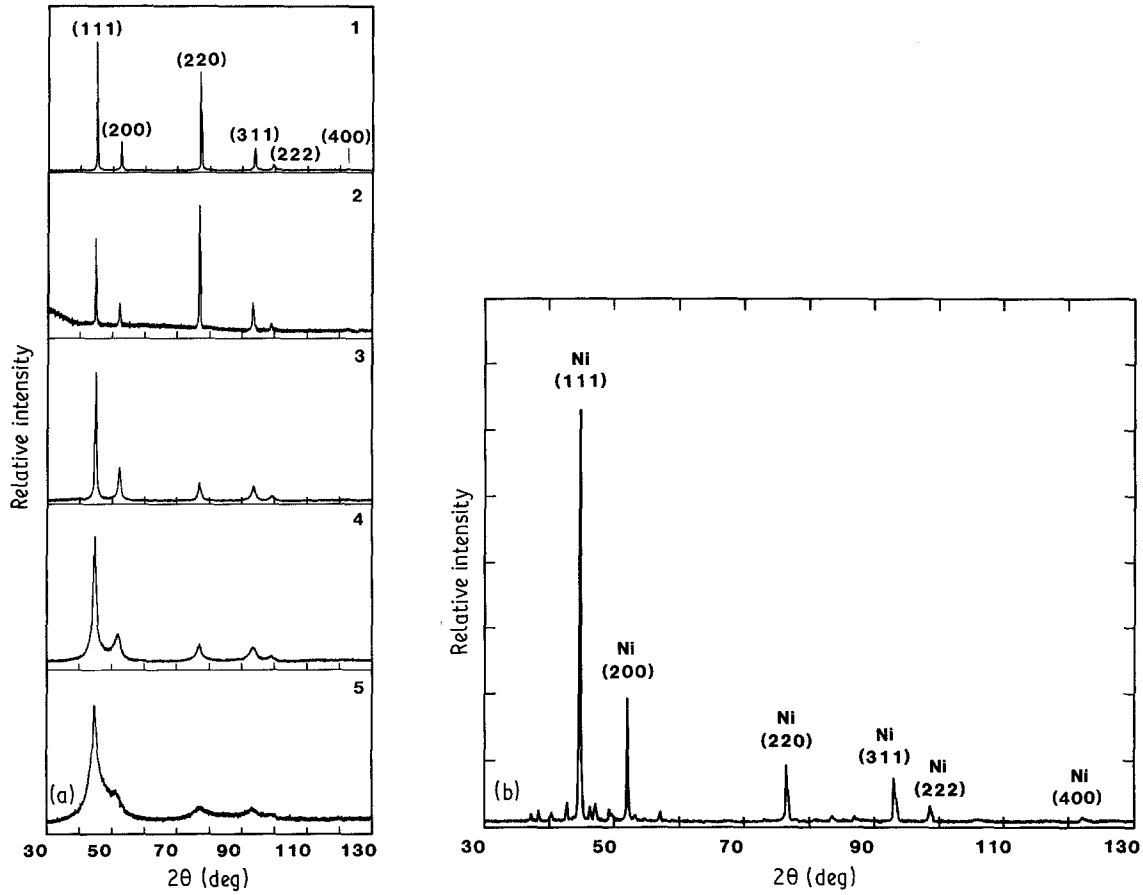

Figure 7 X-ray diffraction data for (a) pure nickel and as-deposited Ni–B alloys: (1) pure Ni, (2) Ni–0.16 % B, (3) Ni–2.6% B, (4) Ni–5.3% B, (5) Ni–13% B, and (b) Ni–13.0 at % B following a 2.5 h anneal at 600° C. The second phase in (b) is Ni_3B. The nickel peaks are indicated in (a) and (b) while the Ni_3B peaks are unlabelled.

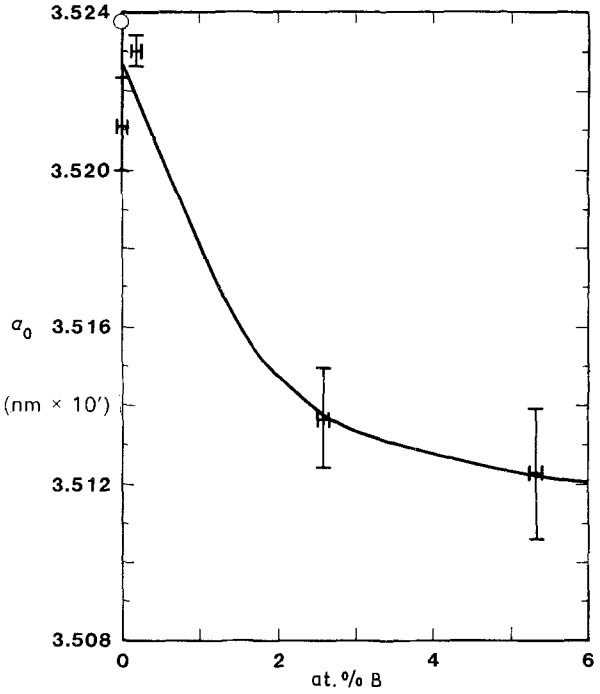

Figure 8 Lattice parameter of Ni–B alloy as a function of boron content. (⊣⊢ data, O literature value for pure nickel.)

agreement with the literature value, 0.352 38 nm [14]. Following an anneal in which the Ni_3B precipitates from the alloy, a_0 returns approximately to the value for pure nickel. For example, a lattice parameter of $0.35219 \pm 1.2 \times 10^{-4}$ nm was found for Ni–2.6 at % B after annealing for 2.5 h at 600° C. The lattice parameters are computed from the diffractometer data shown in Fig. 7a for the as-deposited pure nickel and Ni–B specimens and in Fig. 7b for annealed Ni–13.0 at % B. The lattice parameter data for the as-deposited specimens are listed in Table I and shown in Fig. 8. Lattice parameter data for as-deposited Ni–13.0 at % B are not included because the error in that determination is about 9 times that of the other measurements due to peak broadening.

Skibo and Greulich reported no change in lattice parameter of as-deposited Ni–B alloys containing 0.27–1.08 at % B relative to pure nickel. It was suggested that the boron was incorporated in very fine boride particles at the grain boundaries rather than being in solid solution and hence did not affect the lattice parameter [1]. As shown by Fig. 8, a decrease in a_0 is expected over this composition range but the changes may not be resolvable within the resolution of the technique. In addition, the alloys used in the previous study were prepared commercially. Rather than truly being in the as-deposited condition they may have experienced a thermal cycle which led to precipitation of the boride phase on a fine scale.

An anneal for 1 h at 350° C produced a decreased defect density but no significant grain growth in the Ni–0.16 and 2.6 at % B alloys, as shown for the 2.6 at % B alloy in Fig. 9a. Formation of the Ni_3B intermetallic phase was not detected for these alloys by X-ray or electron diffraction, but was found for the Ni–5.3 and –13 at % B alloys. These results are supported by the precipitation behaviour of these alloys observed by DSC. The temperature of the exotherm corresponding to the precipitation of Ni_3B was measured at heating rates of 5, 10, 20 and 40 K min^{-1} [5]. By extrapolating these data back to a zero heating rate, it appears that isothermal anneals at temperatures as low as 375, 330, and 275° C, respectively for the Ni–2.6, –5.3, and –13.0 at % B specimens, will lead to precipitation of Ni_3B within a few hours. The DSC is not sensitive enough to detect precipitation in the Ni–0.16 at % B material, but this data suggests that the transformation temperature would exceed 400° C.

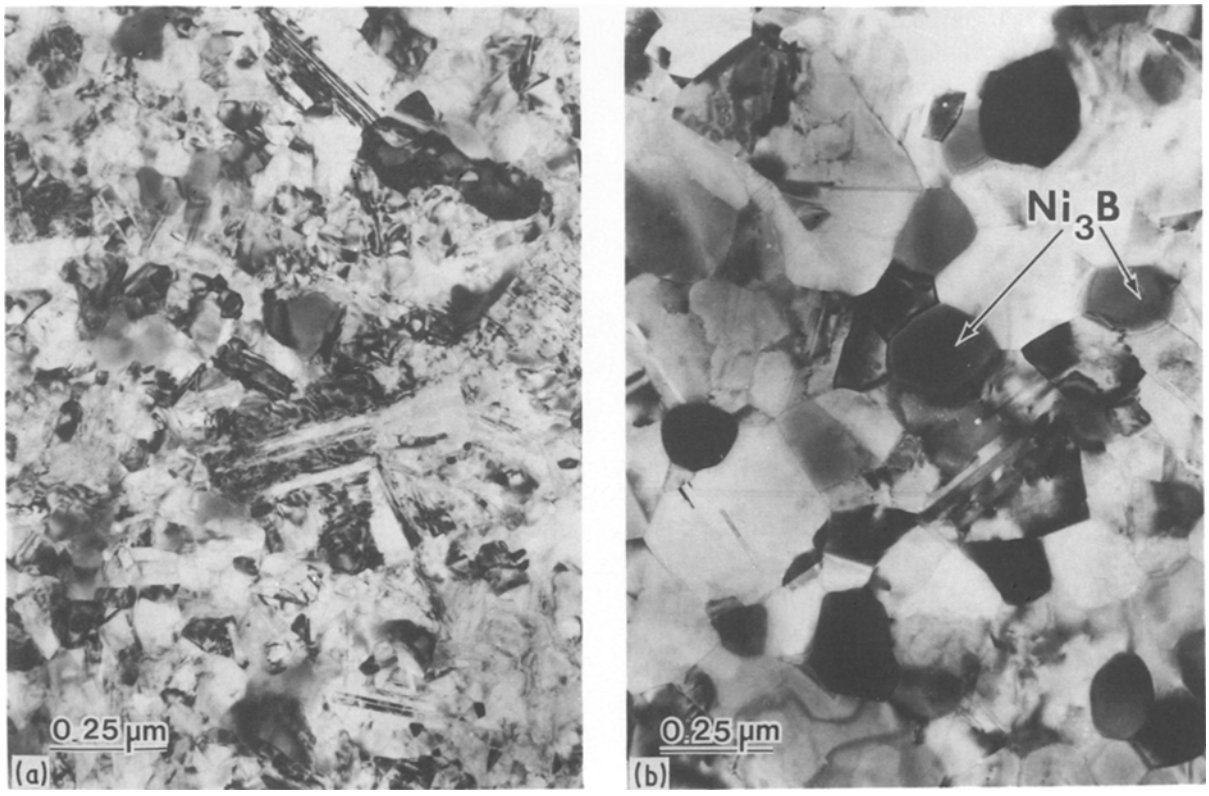

Figure 9 Microstructure of Ni–2.6 at % B after (a) a 1 h anneal at 600° C and (b) following a 600° C, 2.5 h anneal.

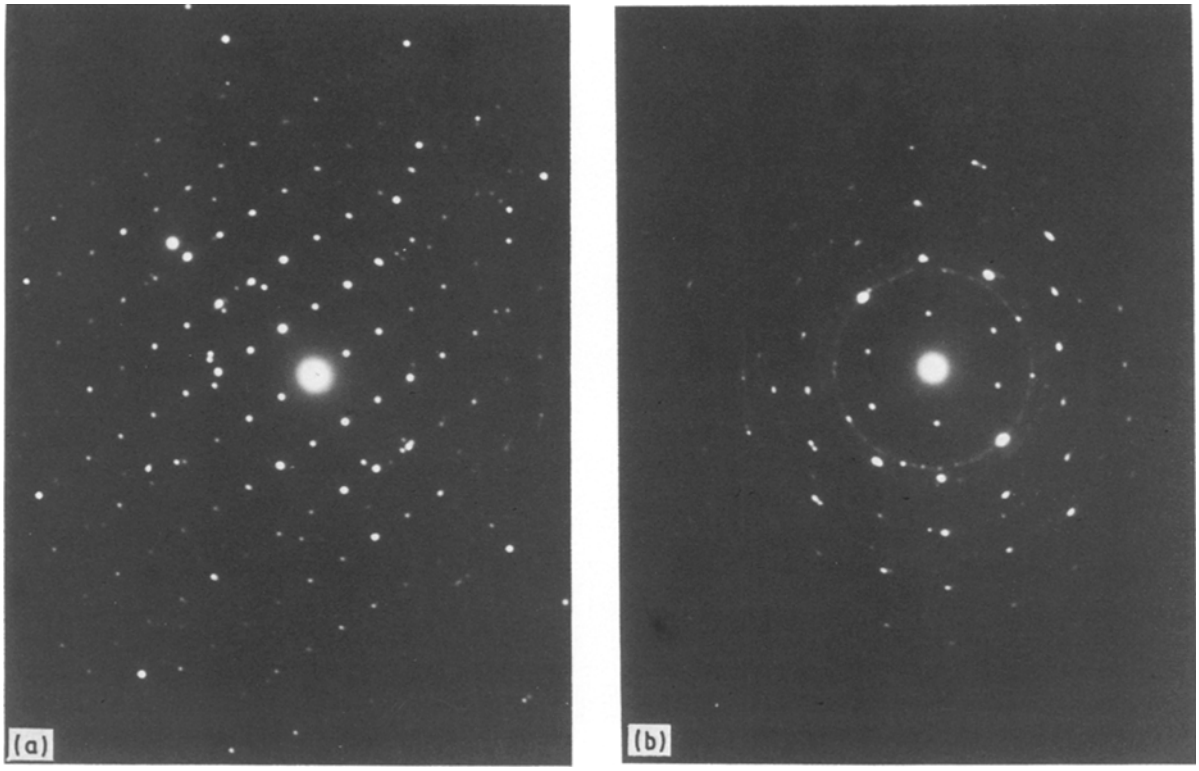

Figure 10 Selected area electron diffraction pattern of (a) $[\bar{1}\,0\,1]$ and (b) $[1\,\bar{2}\,1]$ zones of Ni_3B.

An anneal for 2.5 h at 600° C led to precipitation of Ni_3B, recrystallization and grain growth. The equiaxed microstructure of the Ni–2.6 at % B specimen resulting from the 600° C anneal is shown in Fig. 9b and selected area electron diffraction patterns of the $[\bar{1}\,0\,1]$ and $[1\,\bar{2}\,1]$ zones of Ni_3B appear in Fig. 10. The lack of dislocation and twinning contrast in the Ni_3B grains allows them to be distinguished easily from those of the nickel. The appearance of the microstructure of all of the alloys was about the same after an anneal at 600° C. The primary difference among them was the amount of the Ni_3B phase present, which increased in proportion to the boron content. The post-anneal grain size ranged from about 0.25 μm for the 2.6 at % B alloy to 0.13 μm for Ni–13 at % B material. These results are given in Table I. The X-ray diffractometer scan showing peaks corresponding to both pure nickel and Ni_3B for the Ni–13.0 % B alloy is shown in Fig. 7b.

The Ni_3B intermetallic phase, which is the equilibrium second phase, was identified by both X-ray and electron diffraction. By contrast, Skibo and Greulich [1] reported the formation of the Ni_2B intermetallic phase. In their experiments, the volume fraction of the second phase ($< 5\%$) was insufficient for identification by XRD, and the identification by electron diffraction is more difficult. Further, since no change in the lattice parameter on alloying was observed, it was suggested that boride particles might form in the vapour phase. In that case the boride particles would not necessarily be the Ni_3B phase which is in equilibrium with nickel in the solid phase.

Boron dramatically affects the microhardness of the Ni–B alloys. An optical micrograph showing a cross-section of the layered specimen used to study the effect of boron on the hardness is shown in Fig. 11a with the thickness and composition of the layers indicated. The microhardness, as measured on the Vickers scale with a 100 g load, rises steeply from VHN 200 for the as-deposited pure nickel to approximately VHN 1090 for Ni–5% B. The microhardness data are presented fully in Fig. 11b. The effect of boron on the hardness of the as-deposited Ni–B alloys can be explained in terms of the decreased grain size. The microhardness of these alloys increases in proportion to $d^{-0.5}$, where d is the as-deposited grain diameter from Table I, as shown in Fig. 12. This result is analogous to the Hall–Petch relationship for the dependence of yield strength on grain size [15].

The layered specimens were also annealed for 1 h at temperatures of 350, 600 or 800° C. The considerable drop in microhardness associated with annealing, Fig. 11b, is consistent with the observed recovery, precipitation of Ni_3B and recrystallization with increasing temperature. The microhardness of Ni–13.0 at % B was measured both as-deposited and after annealing at 350° C in another study [2]. The hardness, measured with a 200 g load, was found to increase from VHN 927 for as-deposited Ni–13.0 at % B to VHN 1240 with a 1 h anneal at 350° C. This effect is attributed to precipitation hardening. Skibo and Greulich [1] explored the microhardness of Ni–B alloys containing 0.27–1.08 at % B in the as-deposited condition and after annealing for 4 h at 400, 500, 600 and 800° C. Their results are in qualitative agreement with those of this investigation. They report measurements of Knoop microhardness made with a 500 g load which cannot be directly compared with the Vickers hardness measured with a 100 g load reported in this study.

The tensile strength of CVD Ni–B alloys has been shown to increase with rising boron content for 0.27–1.08 at % B. The elongation of alloys containing 0.27, 0.54 and 0.81 at % B has been determined to be about 9% while that of CVD nickel has been

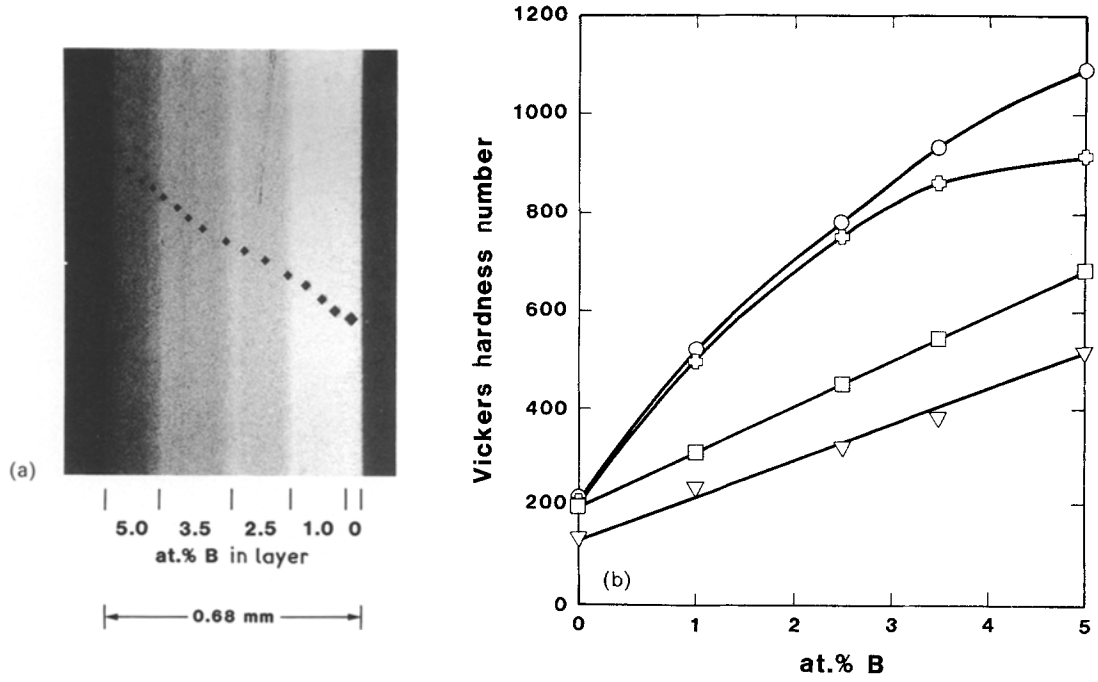

Figure 11 (a) Optical micrograph showing a cross-section of layered specimens used for microhardness measurements. (b) Microhardness as a function of boron content for as-deposited and annealed Ni–B alloys. (○ as-deposited, ⊂⊃ 350° C, 1 h, □ 600° C, 1 h, ▽ 800° C, 1 h.)

measured to be 12.7% [1]. Annealing was found to lower the hardness from which it was inferred that the toughness of the material improves with such treatment. The appropriate tensile tests have not been made for the Ni–B material used in this study. However, the observation from handling these materials to make TEM specimens is that the annealed materials are far more ductile than those in the as-deposited condition.

4. Conclusion

The metalloid, boron, has a profound effect on the microstructure and hardness of CVD Ni–B alloys. Pure nickel deposits are characterized by a bimodal grain size distribution. The large grains are in or near the ⟨0 1 1⟩ orientation and are sometimes found in a pentagonal arrangement. As boron is added the grain size is refined, and ultimately the bimodal size distribution is lost. The defect density and the microhardness rise steeply with boron addition with some attendant loss in ductility. Upon annealing at 350° C or higher, recovery, grain growth and precipitation of the Ni_3B intermetallic phase occur, and in general this leads to a reduction in the hardness. The void content of the deposits was found to increase with boron content. In the Ni–13 at % B alloy large voids form the walls of a cellular structure and smaller voids are found within the cells.

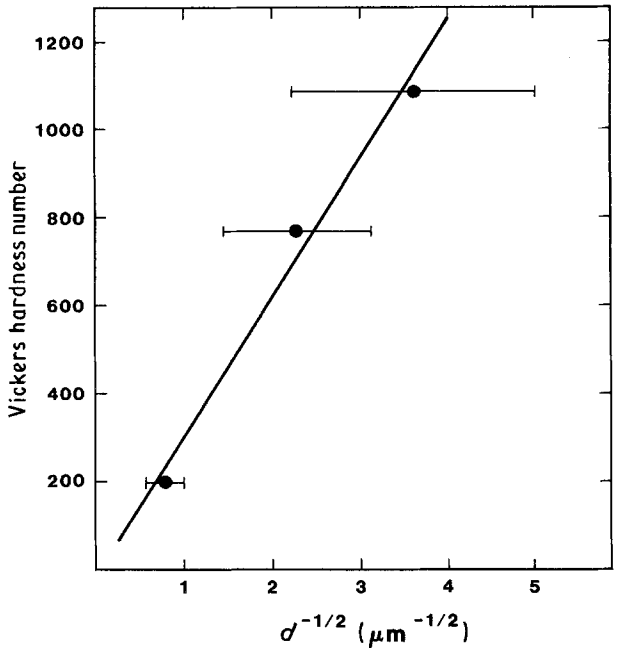

Figure 12 Vickers microhardness plotted $d^{-0.5}$ for as-deposited Ni–B alloys. (—— range of observed grain diameters, ● midpoint of range)

Acknowledgement

The authors gratefully acknowledge the contributions of J. F. Smatana, who assisted with the chemical vapour deposition, M. O. Eatough for the texture analysis and informative discussions concerning the X-ray diffraction results, J. A. Romero, who performed the optical metallography and microhardness testing, and G. C. Nelson and W. B. Chambers, who performed the sputter profiling and ICP analyses, respectively. This work performed at Sandia National Laboratories and Massachusetts Institute of Technology was supported by the US Department of Energy under contract number DE-AC04-76DP00789.

References

1. M. SKIBO and F. A. GREULICH, *Thin Solid Films* **113** (1984) 225.
2. A. W. MULLENDORE and L. E. POPE, *ibid.* **53** (1987) 267.
3. R. P. ELLIOTT, "Constitution of Binary Alloys, First Supplement", (McGraw-Hill, New York, 1965).
4. J.-D. SCHOBEL and N. H. STADELMAIER, *Z. Metallkd.* **56** (1965) 856.
5. E. P. ROTH, A. N. CAMPBELL and A. W. MULLENDORE, Proceedings of the 16th North American Thermal Analysis Society Meeting September 1987, Washington, DC, (North American Thermal Analysis Society) p. 509.

6. C. R. M. GROVENOR, H. T. G. HENTZELL and D. A. SMITH, *Acta. Metall.* **32** (1984) 773.
7. A. N. CAMPBELL, M. J. CARR and J. B. VANDERSANDE, in "Proceedings of the 44th Annual Meeting of the Electron Microscopy Society of America", edited by G. W. Bailey (San Francisco Press, San Francisco, 1986) p. 594.
8. M. J. CARR and W. F. CHAMBERS, *J. Microsc.* **134** (1984) 55.
9. C. Y. YANG, *J. Cryst. Growth* **47** (1979) 274.
10. K. HEINEMANN, M. J. YACAMAN, C. Y. YANG and H. J. POPPA, *ibid.* **47** (1979) 177.
11. S. INO, *J. Phys. Soc. Jpn* **27** (1969) 941.
12. H. T. G. HENTZELL, B. ANDERSSON and S.-E. KARLSSON, *Acta. Metall.* **31** (1983) 2103.
13. B. A. MOVCHAN and A. V. DEMCHISHIN, *Fizika Metall.* **28** (1977) 83.
14. JCPDS File No. 4-850.
15. A. G. GUY and J. J. HREN, "Elements of Physical Metallurgy", 3rd Edn (Addison-Wesley, Reading, MA, 1974) p. 466.

Received 23 November 1987
and accepted 3 March 1988